doi:10.2533/chimia.2022.316 Chimia 76 (2022) 316–321

The Effect of the Molecular Dipole and Quadrupole Moments on Ion–Molecule Reaction Rates near 0 K

Valentina Zhelyazkova*

SCS-Metrohm Award for the best oral presentation in Physical Chemistry

Abstract: We review the results of our recent experimental and theoretical studies of gas-phase ion–molecule reactions involving the He^+ ion at low collision energies (E_{coll}), in the $k_B \cdot (0 - 40)$ K range. To avoid heating of the ions by stray electric fields, the reactions are studied within the orbit of a Rydberg electron. We reach collision energies down to ~0 K by employing a merged-beam setup. In the case of a molecule with a dipole moment (*e.g*. ammonia), we observe a strong enhancement of the measured reaction yield with decreasing E_{coll}. This enhancement is attributed to rotational states which experience linear negative Stark shifts in the electric field of the ion. When the molecule has no dipole moment but a negative quadrupole moment (*e.g.* N_2), we observe a suppression of the total reaction yield at the lowest collision energy. Our results are interpreted with the aid of an adiabatic-channel model.

Keywords: Cold ion–molecule chemistry · Dipole moment · Quadrupole moment · Rydberg helium

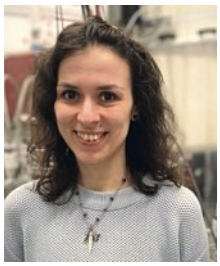

Valentina Zhelyazkova received a BSc in Physics from Trinity College, CT. She was then awarded an MRes in Controlled Quantum Dynamics (2010) and a PhD (2014) degrees from Imperial College London. During her PhD work, she demonstrated laser cooling and slowing of a supersonic beam of calcium fluoride radicals. As a postdoctoral researcher at UCL, she gained experience in the preparation and manipulation of Rydberg atoms for applications in spectroscopy and studies of resonant energy transfer with polar molecules. Since 2017, she has been working in the group of Prof. Frédéric Merkt at ETH Zürich studying ion–molecule reactions in the gas phase at low collision energies.

1. Introduction

Ion–molecule reactions can be fast, barrierless and exothermic, proceeding with high rate coefficients even at low temperatures. These reactions play a key role for the synthesis of molecules in the cold and tenuous environment of the interstellar medium, enabling reaction chains that lead to the formation of polyatomic species in dark molecular clouds (with temperatures in the 10–50 K range).[1,2] The rate coefficients and product branching ratios of ion–molecule reactions are necessary as input parameters for kinetic models of the chemical reaction cycles in these clouds.

Ion–molecule reactions are challenging to study at temperatures below ~10 K because stray electric fields induce heating of the ions. A difference of only ~1 mV in the electric potential across the reaction zone is already sufficient to impart a kinetic energy of $\sim k_B \cdot 12$ K to a singly-charged ion. Effects of the interactions between the ion and the multipole moment of the molecule are expected to become significant at low temperatures, and have been studied theoretically.[3,4] Below 1 K, quantum phenomena may begin to emerge.[5–7]

We have developed an experimental technique to study ion–molecule reactions at very low temperatures (down to ~200 mK) by replacing the ion with an atom or molecule in a Rydberg state of high principal quantum number n.[8–16] The Rydberg electron moves on an orbit of large radius ($\propto n^2$, ~50 nm for $n = 30$) and does not affect the reaction of the ion core with the neutral molecules located within the electron orbit, but shields it from stray electric fields.[14,17–19] We use helium Rydberg atoms [referred to as He(n)] which are merged with a supersonic beam of the molecule of interest using a Rydberg-Stark decelerator and deflector.[8,12,20] The collision energy can be varied by changing the velocity of the He(n) atoms with the surface deflector while the velocity of the molecular beam (referred to as the ground-state (GS) beam) is kept constant. With this approach, one can achieve very low relative collision energies in the moving centre-of-mass reference frame of the colliding Rydberg-atom–molecule pair by exploiting the velocity dispersion taking place in the beam of neutral molecules, as was exploited recently in studies of Penning ionization reactions.[21,22]

2. Experimental Setup

The experimental setup is described in detail in refs. [12] and [13]. Briefly, two supersonic beams, one for the helium atoms and one for GS molecules of interest, are produced using two home-built short-pulse valves (pulse duration ~20 µs). The copper body of the helium valve, tilted by 5° with respect to the vertical, is cooled by a two-stage pulse-tube cryo-cooler. The He valve is temperature-stabilised to either 66.0 ± 0.5 K or 100.0 ± 0.5 K, resulting in a mean forward velocity of the helium beam of ~860 and ~1040 m/s, respectively.

A pulsed electric potential (~500 V) applied to a ring electrode at the He valve orifice and a tungsten filament are used to produce the $(1s)(2s)\ ^3S_1$ metastable state in helium (referred to as He^*) in an

*Correspondence: Dr. V. Zhelyazkova, E-mail: valentina.zhelyazkova@phys.chem.ethz.ch
Laboratory of Physical Chemistry, ETH Zürich, CH-8093 Zürich, Switzerland

electric discharge.[12,23] After passing through two skimmers, the He^* beam is intersected at right angles by the frequency-tripled output of an Nd:YAG-pumped commercial dye laser (excitation wavelength ~260 nm, repetition rate 25 Hz), in the presence of a dc electric field. A one-photon excitation is driven to a low-field-seeking Rydberg-Stark state (n,k,m) = (30,21,0) just below the Inglis-Teller field (n and m are the principal and magnetic quantum numbers, respectively, k = –(n–|m|–1):2:(n–|m|–1), and the Inglis-Teller field is the field at which the Stark manifolds of neighbouring n values start overlapping).[24]

After excitation, the He(n) Rydberg atoms are captured in quadrupole traps formed above the surface of a 50-electrode Rydberg-Stark deflector and decelerator (see Fig. 1) by applying the appropriate electric potentials to several sets of its electrodes. By applying sinusoidally-varying potentials, the trapped cloud of Rydberg atoms (of radius ~ 0.5 mm and length ~ 3 mm) can be guided along the surface of the deflector, and accelerated or decelerated to a final velocity (ν_{Ryd}) in the 700–1200 m/s range.[12,13,25] We estimate that ~100 Rydberg atoms reach the reaction region after deflection at each experimental cycle.

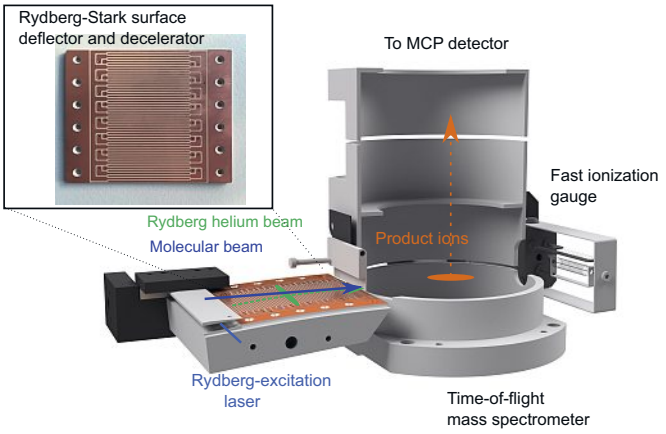

Fig 1. A schematic diagram of the merged-beam setup with the 50-electrode surface Rydberg-Stark deflector and decelerator. The reaction product ions are collected in a time-of-flight mass spectrometer.

The GS beam valve is operated with a pure gas containing the molecules of interest. It is temperature-stabilised to produce beams with mean forward velocities of $\nu(NH_3)$ = 1190 m/s, $\nu(ND_3)$ = 1170 m/s and $\nu(N_2)$ = 860 m/s, determined using two fast-ionization gauges.[13]

After being merged with the molecules from the GS beam, the Rydberg atoms enter a time-of-flight mass spectrometer, where the reaction product ions are extracted and collected on a microchannel plate (MCP) detector (schematically depicted in Fig. 1). The reaction-observation window is typically 7 µs.

The collision energy of the reaction is given by Eqn. (1):

$$E_{\rm coll} = \frac{1}{2}\mu v_{\rm rel}^2 = \frac{1}{2}\mu(v_{\rm Ryd} - v_{\rm GS})^2, \qquad (1)$$

where µ is the reduced mass of the helium atom and the molecule, and ν_{GS} is the velocity of the molecule. In the experiment, we change E_{coll} by varying ν_{Ryd} with the appropriate potentials applied to the electrodes of the surface deflector, while ν_{GS} is kept fixed.[12,13]

3. The Modified Langevin Ion–Molecule Interaction Potential

Usually, ion–molecule reactions are described by the Langevin model[26] in which the long-range interaction potential for the capture is given by Eqn. (2):

$$V_{\rm L}(R) = \frac{L^2}{2\mu R^2} - \frac{(Ze)^2\alpha'}{8\pi\epsilon_0 R^4}, \qquad (2)$$

where R is the separation between the ion and the molecule, L is the angular momentum of the colliding pair, (Ze) is the charge of the ion, $\alpha' = \alpha/(4\pi\varepsilon_0)$ is the polarizability volume of the molecule and α is the polarizability. The first term in Eqn. (2) is the centrifugal potential of the collision, while the second term describes the interaction between the ion and the induced dipole of the polarizable molecule. In the Langevin model, the reaction is assumed to proceed with unit probability if the collision energy is high enough to overcome the centrifugal potential energy barrier (this is known as the capture condition).

In the original Langevin model, the molecule is assumed to be a polarizable object, without any intrinsic charge distribution. Eqn. (2) leads to an expression for the Langevin capture rate coefficient, k_L, which is temperature- and collision-energy-independent and given by Eqn. (3):

$$k_{\rm L} = \sigma v_{\rm rel} = \sqrt{\frac{\pi\alpha'(Ze)^2}{\epsilon_0\mu}}, \qquad (3)$$

where $\sigma = \pi b_{max}^2$ is the reaction cross section (b_{max} is the maximum impact parameter for which the reaction still takes place).

In the presence of a molecular dipole or quadrupole moments, however, the interaction potential in Eqn. (2) must be modified in order to include the Stark shift, ΔE_i, of the molecule in rotational state i as it experiences the electric field of the ion.[13] Assuming that the molecule remains in its original quantum state as it approaches the ion, as in the adiabatic-channel model,[10,11] the total interaction potential is then given by Eqn (4):

$$V_{{\rm int},i}(R) = V_{\rm L}(R) + \Delta E_i. \qquad (4)$$

The inclusion of the Stark shift in Eqn. (4) can significantly modify the maximally-allowed angular momentum for each collision energy, $L_{max} = \mu v_{rel} b_{max}$, and lead to a reaction rate coefficient which is strongly rotational-state- and collision-energy dependent, given by Eqn. (5):

$$k_i(E_{\rm coll}) = \frac{\pi L_{{\rm max},i}^2}{\sqrt{2\mu^3 E_{\rm coll}}}. \qquad (5)$$

4. Ion-dipole Enhancement of the Ion–Molecule Reaction Rate Coefficients at Low Energies

The results presented in this section are presented in more detail in ref. [13]. Shown in Fig. 2 are the reaction product-ion yields and calculated capture rate coefficients of the $He^+ + NH_3$ and $He^+ + ND_3$ reactions, for collision energies in the k_B·(0–40) K range.[13] The insets of Fig. 2 show the measured product-ion time-of-flight

mass spectra with the Rydberg excitation laser turned on (black) and off (blue). The time-of-flight mass spectra recorded with the Rydberg excitation laser turned off exhibit peaks corresponding to products of Penning-ionization processes involving He^* and ammonia and He^* and background water present in the vacuum chamber. We can assign these peaks to OH^+, H_2O^+, NH_3^+ and ND_3^+ ions. When the Rydberg excitation laser is turned on, additional peaks appear in the time-of-flight mass spectra. The first and most prominent peak corresponds to He^+ ions originating from He(n) atoms which have been field-ionized during the ion-extraction pulse. A considerable amount of He(n) is present even when the GS beam is on, because only a small amount (less than ~0.4%) of the Rydberg atoms takes part in the chemical reactions.[12–16] In order to identify the ion–molecule reaction product ions for each reaction, the Penning-ionization contribution to the recorded time-of-flight mass spectra is subtracted.

The product ions of the $He^+ + NH_3$ (ND_3) reaction detected in our experiments are: NH^+(ND^+) and NH_2^+(ND_2^+), with a branching ratio of ~1:6 (~1:4).[13] The total reaction product yield of each reaction, displayed as the green circles with error bars in Fig. 2, is obtained by summing the contributions from the two product ion signals integrated over the green windows indicated in the insets. The vertical error bars in Fig. 2 correspond to the standard deviations of five consecutive measurements, each consisting of the average of 1000 experimental cycles. The horizontal error bars indicate the spread of collision energies, ΔE_{coll}, for each value of E_{coll} given by Eqn. (6)[12]:

$$\Delta E_{\mathrm{coll}} = \Delta E_{\mathrm{res}} + 2\sqrt{E_{\mathrm{coll}}}\sqrt{\Delta E_{\mathrm{res}}}. \qquad (6)$$

The term ΔE_{res} in Eqn. (6) reflects the experimental resolution at zero collision energy and is determined by the velocity spread around the centre velocity (v_{Ryd}) of the Rydberg atoms released from the quadrupole traps above the surface of the deflector. Typical values of ΔE_{res} are in the k_B·(150–300) mK range.

Both data sets presented in Fig. 2 show an increase of the reaction yields with decreasing values of E_{coll}. This increase is particularly strong below ~k_B·5 K. Also shown in Fig. 2, as orange and purple circles, are the calculated collision-energy-dependent capture rate coefficients averaged over the rotational states in ammonia which are populated in the supersonic beam, assuming a rotational temperature of 6 K. The black lines represent the calculated averaged capture rate coefficients with the effect of the experimental resolution included, as described in ref. [12]. For both reactions, the calculation describes the experimental data very well. The total integrated product ion signals in each data set were scaled to match the value of the calculated average capture rate coefficients at the minimal experimentally resolvable collision energy. The values of ΔE_{res} and the rotational temperature of the molecules, T_{rot}, were varied to obtain the best agreement with the experimental data. Following this procedure, we obtain the values ΔE_{res} = 200 mK and T_{rot} = 6 K. At the lowest collision energy accessible in the experiment, the calculated capture rates of the reactions reach values of ~16 k_L in He^+ + NH_3 and ~21 k_L in He^+ + ND_3, indicating a strong deviation from Langevin behaviour.

The observed enhancement of the reaction yields with decreasing E_{coll} arises from the dipole moment of ammonia (1.48 D),[27] and in particular from rotational states which have the largest negative Stark shifts [see Eqn. (4)]. Although NH_3 and ND_3 have the same dipole moment, the observed enhancement is more pronounced in ND_3 compared to NH_3. This is because of the smaller (by a factor of ~2) rotational constants in ND_3, which induce stronger J – mixing and Stark shifts, and, to a lesser degree, the smaller separation between the umbrella-motion-tunnelling doublets in ND_3 (~ 0.053 cm^{-1})[28] compared to NH_3 (~ 0.79 cm^{-1}).[29] Both of these effects lead to rotational states which are shifted to lower energies in an electric field in ND_3 compared to NH_3.

The rotational constants of NH_3 and ND_3 ($A(NH_3) = B(NH_3)$ = 9.444 cm^{-1} and $C(NH_3)$ = 6.196 cm^{-1},[29] and $A(ND_3) = B(ND_3)$ = 5.143 cm^{-1} and $C(ND_3)$ = 3.125 cm^{-1}[28]) mean that only *ortho* and *para* levels with $J \leq 1$ and $|K| \leq 1$ are significantly populated at the rotational temperature of the supersonic source (~ 6 K) in both isotopologues. In addition, according to nuclear-spin statistical effects and assuming nuclear-spin-conservation in the supersonic beam, the ratio of states with $K = 0$ to states with $|K| = 1$ is 1:1 in NH_3 and 11:16 in ND_3.[13] The Stark shifts experienced by rotational states with $J \leq 1$ and $|K| \leq 1$ are thus crucial for the observed overall collision-energy dependence of the reaction yields.

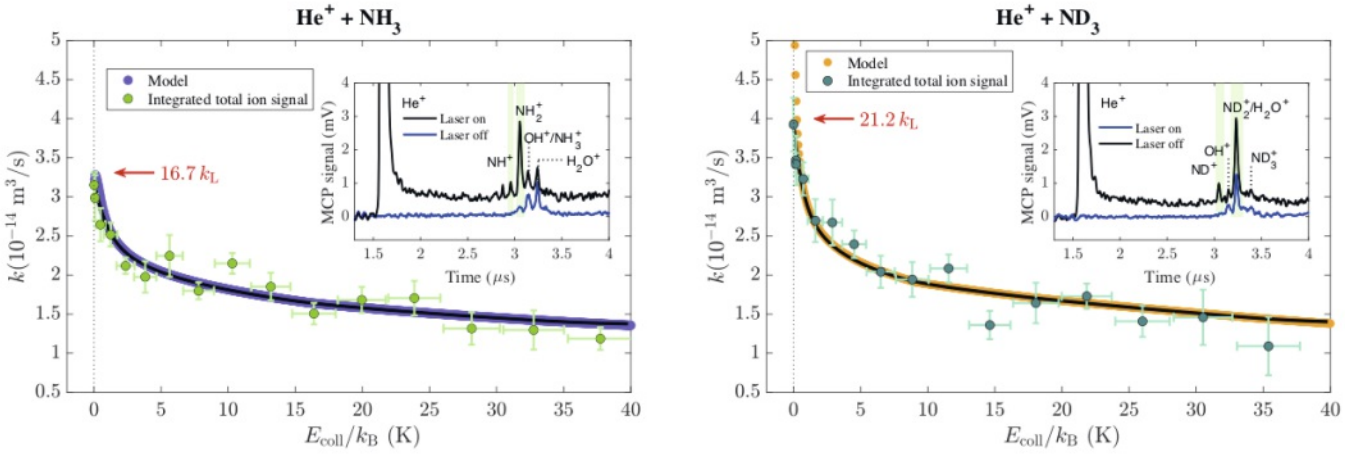

Fig. 2. Total measured reaction product-ion yield for the He^+ + NH_3 (left panel, light green circles with error bars) and He^+ + ND_3 (right panel, dark green circles with error bars) reactions, as a function of the collision energy. The purple and orange circles are the calculated capture rate coefficients of the two reactions, averaged over the rotational state population of the ammonia molecules produced in the supersonic beam, assuming a rotational temperature of 6 K. The black lines represent the calculated capture rate coefficients with the finite experimental energy resolution included. The insets show the measured product-ion time-of-flight mass spectra after a reaction time of 7 μs and recorded with v_{Ryd} = 1050 m/s. The figure is adapted from Figs. 3 and 4 of ref. [13].

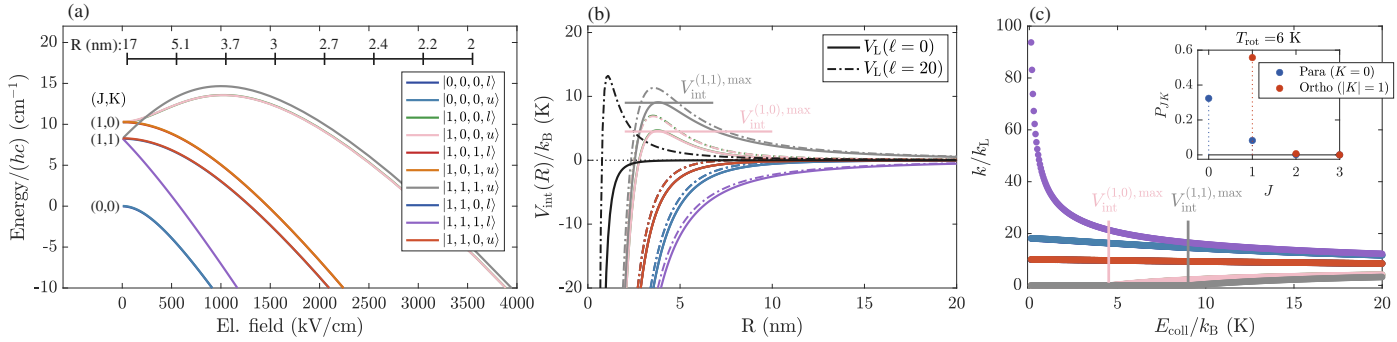

Fig. 3. The calculated rotational-state dependent Stark energies, interaction potentials and capture rate coefficients for the $He^+ + ND_3$ reaction. (a) The calculated Stark shifts of rotational levels in ND_3 with $J \leq 1$ and $|K| \leq 1$. The legend refers to the $|JKM/u\rangle$ label of the states, with l and u indicating the lower and upper component of the inversion doublet (not resolvable on this scale). The top horizontal bar indicates several selected distances to the ion. (b) The interaction potentials for the rotational states shown in (a) for $l = 0$ (solid coloured lines) and $l = 20$ (dash-dotted coloured lines), and the respective Langevin potentials V_L in black solid and black dash-dotted lines, respectively. (c) Calculated rotational-state- and collision-energy-dependent capture rate coefficients. The inset shows the rotational state population in ND_3 at a rotational temperature of 6 K.

Displayed in Fig. 3 are the calculated rotational-state-dependent Stark energies, interaction potentials and reaction rate coefficients in ND_3 for rotational states with $J \leq 1$ and $|K| \leq 1$. The rotational states can be categorised in three groups, according to the Stark shifts they experience, as: (A) strongly high-field-seeking states which experience negative linear Stark shifts at low fields – *e.g.* states with $|KM| = 1$ correlating to the lower component (l) of the umbrella-motion tunnelling doublet [Fig. 3(a)]. These states are subject to strongly enhanced rate coefficients with decreasing collision energy, reaching values of ~ 94 k_L at $E_{coll} = k_B \cdot 100$ mK [Fig. 3(c)]; (B) high-field-seeking states subject to a quadratic Stark shift at low fields, *e.g.* some of the states with $|KM| = 0$ [Fig. 3(a)]. These states exhibit only weak rate enhancements, reaching values of ~ $(10 - 20)k_L$ at the lowest collision energies [Fig. 3(c)]; and (C) low-field-seeking states at low electric fields, *e.g.* the states with $J = 1$ and $|K| = |M|$ in Fig. 3(a). These states exhibit rate coefficients which are completely suppressed at the lowest collision energies and only start to grow for $E_{coll} > V_{int}^{max}$ [see Fig. 3 (b) and (c)]. Displayed in Fig. 3(b) are the total interaction potentials V_{int} (in colour), as well as the pure Langevin potential for the $He^+ + ND_3$ reaction (in black) for a head-on-collision ($l = 0$, $L = \hbar\sqrt{[l(l+1)]}$ in solid lines and for a collision with $l = 20$ in dash-dotted lines. The height of the potential energy barrier in the Langevin potential for $l = 20$ is completely suppressed in high-field-seeking states of types (A) and (B). States of type (C), on the other hand, experience a potential-energy barrier [designated as V_{int}^{max} in Fig. 3(b)] even for collisions with $l = 0$. These states are only reactive for collision energies which are sufficiently high to overcome the potential energy barrier V_{int}^{max} [Fig. 3(c)]. Because the enhancement of the capture rate coefficient with decreasing energy is so striking in states of type (A), these states dictate the overall behaviour of the total rate coefficient, averaged over the population of rotational states, even though these states comprise only 19.6% (in ND_3) and 15.1% (in NH_3) of the total population at $T_{rot} = 6$ K.

5. Ion-quadrupole-induced Suppression of the Reactivity at Low Collision Energies

The results presented in this section were presented in more detail in ref. [15]. Shown in Fig. 4 is the total measured product ion yield (green circles with error bars) for the $He^+ + N_2$ reaction, together with the calculated averaged capture rate coefficients, for a rotational temperature of 7.5 K, without (purple circles) and with (black line) the experimental resolution included, as explained above, for collision energies in the $k_B \cdot (0 - 12)$ K range. The ion–molecule reaction product ions detected in this reaction are N^+ and N_2^+, with a branching ratio of ~1:1 (see inset of Fig. 4). The experimental and calculated energy-dependent rate coefficients show a suppression of the reaction yield with decreasing energy, with the total measured product-ion signal at the lowest collision energy being ~30% less than that at ~$k_B \cdot 10$ K.

Since the nitrogen molecule is homonuclear, it has no dipole moment in its ground electronic state. The observed suppression of the reaction product, however, can be explained with the rotational-state dependent Stark shifts originating from the negative value of the Q_{zz} component of the quadrupole moment tensor ($Q_{zz}(N_2) = -1.306$ DÅ[5]). The negative value of Q_{zz} corresponds to an electronic configuration in which there is excess positive charge ($+2|\delta|$) near the N_2 molecule centre of mass and excess negative charges ($-|\delta|$) near each nitrogen atom. This charge distribution results from the one σ and two π bonds comprising the triple bond of N_2.

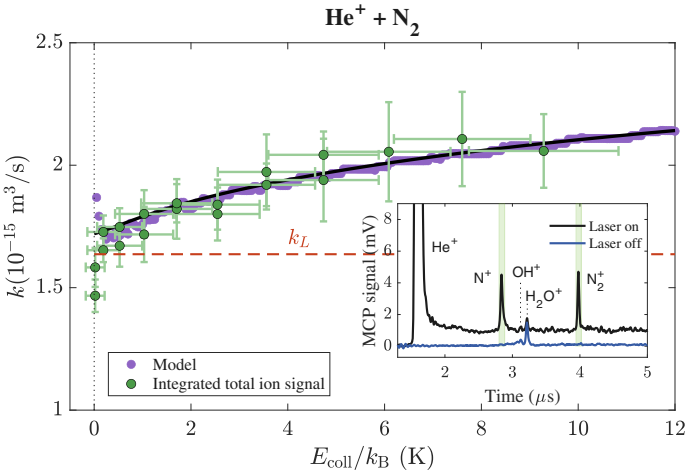

Fig. 4. Measured total product-ion yield for the $He^+ + N_2$ reaction (green circles with error bars) as a function of the reaction collision energy. Purple circles: the calculated capture rate coefficients, averaged over the rotational state population in the supersonic beam at a rotational temperature of 7.5 K. Black lines: the calculation with the finite experimental resolution included. The inset shows the measured product-ion time-of-flight mass spectra after a reaction time of 7 μs and recorded with v_{Ryd} = 1040 m/s. Adapted from Figs. 2 and 3 of ref. [15].

The ion-quadrupole interaction ($\propto R^{-3}$) is much weaker than the ion-dipole interaction ($\propto R^{-2}$), and thus the values of the calculated capture rate coefficients for the $He^+ + N_2$ reaction are much closer to k_L [see Figs. 4 and 5(c)] than those for the $He^+ + N(H/D)_3$ reactions.

Displayed in Fig. 5 are the Stark shifts in N_2 (a), calculated as described in refs. [13] and [15], the interaction potentials for an $l = 0$ collision with a He^+ ion (b), and the calculated rotational-state- and collision-energy-dependent capture rate coefficients (c), for states with $J \leq 2$, which are the only significantly-populated states at the rotational temperature of the supersonic source (here, 7.5 K). States with a maximal value of $|M|$, *e.g.* the $(J, |M|) = (1,1)$ and (2,2) states, result in a configuration in which the positive charge near the molecular centre is exposed to the positive charge of the ion (see Fig. 5 from ref. [15]), resulting in an overall repulsive potential. These states are thus low-field-seeking at low electric fields, are characterized by interaction potentials with potential-energy barriers even for a collision with $l = 0$ [designated as V_{int}^{max} in Fig. 5(b)], and have rate coefficients which are zero for $E_{coll} < V_{int}^{max}$ [Fig.5 (c)]. In states with $M = 0$, on the other hand, it is the negative partial charges located on the N atoms which are exposed to the positively charged He^+ ion, resulting in an interaction potential which is more attractive than V_L. The (0,0) state has no quadrupole moment to first order, but acquires one through mixing with the (2,0) state. The (0,0) state is thus only slightly more attractive than V_L, and exhibits a rate coefficient which starts at a value of k_L at the lowest energies and increases to $\sim 1.5 k_L$ at $E_{coll} = k_B \cdot 12$ K. The other states with $M = 0$, on the other hand, have rate coefficients which increase at the lowest values of E_{coll}.

The nuclear-spin statistics of $^{14}N_2$ dictate that 2/3 of the molecules are in states with $J = 0, 2, 4, \ldots$ (*ortho*) and 1/3 in states with $J = 1, 3, 5, \ldots$ (*para*). The behaviours of the total averaged capture rate coefficients in the $He^+ + N_2$ reaction is thus determined by the (0,0) and (1,1) states, which comprise respectively ~ 44% and ~ 21% of the total population at a rotational temperature of 7.5 K.

6. Conclusions

We have developed an experimental technique to measure relative reaction rate coefficients of reactions between the He^+ ion and several small molecules (*e.g.* CH_3F,[12] NH_3,[13] CO,[14] N_2[15] and CH_4[16]), within the orbit of a Rydberg electron. By using a merged-beam setup, we are able to access collision energies in the $\sim k_B \cdot (0–40)$ K range. We observe a pronounced deviation from the temperature- and collision-energy-independent Langevin capture rate coefficients k_L for molecules with a dipole or quadrupole moments. In the case in which the molecule has a significant dipole moment (*e.g.* CH_3F and NH_3), we observe a strong enhancement of the reaction rate coefficients at the lowest collision energies studied ($\sim k_B \cdot 200$ mK), reaching values more than an order of magnitude larger than k_L.[12,13] This enhancement is attributed to molecular rotational states which experience strong negative and linear Stark shifts in the electric field of the ion. When the molecule has no significant dipole moment, but a negative quadrupole moment (e.g., N_2 and CO), a pronounced suppression of the total product-ion yield is observed at the lowest collision energies.[14,15]

The adiabatic-capture theory used to aid the interpretation of the results shows excellent agreement with the experimental data, suggesting that this model is adequate to describe the collision-energy-dependence of the rate coefficients down to $\sim k_B \cdot 200$ mK. By also calculating the thermal reaction rate coefficients[13,15,16] and using the measured values of the absolute thermal rate coefficients of ion–molecule reactions available in the literature for low temperatures (in the 10–50 K range), we can also determine the reaction probability (which we estimate to be ~ 60–70% for the $He^+ + N_2$ reaction[15] and ~40% for the $He^+ + NH_3$ reaction).[13] Our low-energy measurements, together with the developed model, make it possible to predict the absolute thermal rate coefficients of numerous ion–molecule reactions at low temperatures which are relevant for astrophysical kinetic models.

Acknowledgements

V. Z. acknowledges the crucial contributions of Fernanda B. V. Martins and Dr. Matija Žeško to the acquisition of the experimental data presented, and thanks Prof. Frédéric Merkt for the invaluable discussions and guidance, and Josef A. Agner and Hansjürg Schmutz for the technical support. This work is supported financially by the SNSF (Grant No. 200020B-200478) and by the European Research Council through the ERC advanced grant (Grant No. 743121) under the European Union's Horizon 2020 research and innovation programme.

Received: February 14, 2022

[1] T. P. Snow, V. M. Bierbaum, *Annu. Rev. Anal. Chem.* **2008**, *1*, 229. https://doi.org/10.1146/annurev.anchem.1.031207.112907
[2] D. Smith, *Chem. Rev.* **1992**, *92*, 1473, https://doi.org/10.1021/cr00015a001
[3] J. Troe, *Chem. Phys.* **1987**, *87*, 2773, https://doi.org/10.1063/1.453701
[4] D. C. Clary, *Annu. Rev. Phys. Chem.* **1990**, *41*, 61, https://doi.org/10.1146/annurev.pc.41.100190.000425
[5] E. I. Dashevskaya, I. Litvin, E. E. Nikitin, J. Troe, *J. Chem. Phys.* **2004**, *120*, 9989, https://doi.org/10.1063/1.1724822
[6] B. Gao, *Phys. Rev. A* **2011**, *83*, 062712, https://dx.doi.org/10.1103/PhysRevA.83.062712
[7] E. Vogt and G. H. Wannier, *Phys. Rev.* **1954**, *95*, 1190, https://doi.org/10.1103/PhysRev.95.1190

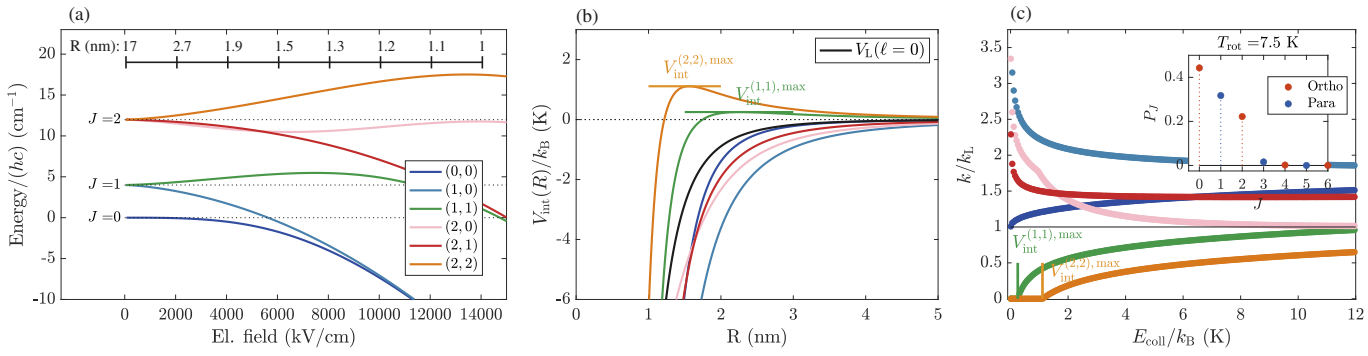

Fig. 5 The calculated rotational-state dependent Stark energies, interaction potentials and capture rate coefficients for the $He^+ + N_2$ reaction. (a) The calculated Stark shifts of the rotational levels with $J \leq 2$ in N_2. (b) Interaction potentials for the rotational states shown in (a) for $l = 0$ (solid coloured lines) and the pure Langevin potential V_L in black. (c) The calculated rotational-state dependent capture rate coefficients. The inset shows the rotational state population in $^{14}N_2$ at a rotational temperature of 7.5 K.

[8] P. Allmendinger, J. Deiglmayr, O. Schullian, K. Höveler, J. A. Agner, H. Schmutz, F. Merkt, *Chem. Phys. Chem.* **2016**, *17*, 3596, https://doi.org/10.1002/cphc.201600828
[9] P. Allmendinger, J. Deiglmayr, K. Höveler, O. Schullian, F. Merkt, *J. Chem. Phys.* **2016**, *145*, 244316, https://doi.org/10.1063/1.4972130
[10] K. Höveler, J. Deiglmayr, J. A. Agner, H. Schmutz, F. Merkt, *Phys. Chem. Chem. Phys.* **2021**, *23*, 2676, https://doi.org/10.1039/D0CP06107G
[11] K. Höveler, J. Deiglmayr, F. Merkt, *Mol. Phys.* **2021**, *119*, e1954708, https://doi.org/10.1080/00268976.2021.1954708
[12] V. Zhelyazkova, F. B. V. Martins, J. A. Agner, H. Schmutz, F. Merkt, *Phys. Rev. Lett.* **2020**, *125*, 263401, https://doi.org/10.1103/PhysRevLett.125.263401
[13] V. Zhelyazkova, F. B. V. Martins, J. A. Agner, H. Schmutz, F. Merkt, *Phys. Chem. Chem. Phys.* **2021**, *23*, 21606, https://doi.org/10.1039/D1CP03116C
[14] F. B. V. Martins, V. Zhelyazkova, C. Seiler, F. Merkt, *New J. Phys.* **2021**, *23*, 095011, https://doi.org/10.1088/1367-2630/ac231d
[15] V. Zhelyazkova, F. B. V. Martins, M. Žeško, F. Merkt, *Phys. Chem. Chem. Phys.* **2022**, https://doi.org/10.1039/D1CP04798A
[16] V. Zhelyazkova, F. B. V. Martins, F. Merkt, *Phys. Chem. Chem. Phys.*, submitted.
[17] S. T. Pratt, J. L. Dehmer, P. M. Dehmer, W. A. Chupka, *J. Chem. Phys.* **1994**, *101*, 882, https://doi.org/10.1063/1.467741
[18] E. Wrede, L. Schnieder, K. Seekamp-Schnieder, B. Niederjohann, K. H. Welge, *Phys. Chem. Chem. Phys.* **2005**, *7*, 1577, https://doi.org/10.1039/B417440B
[19] M. Matsuzawa, *Phys. Rev. A* **2010**, *82*, 054701, https://doi.org/10.1103/PhysRevA.82.054701
[20] P. Allmendinger, J. Deiglmayr, J. A. Agner, H. Schmutz, F. Merkt, *Phys. Rev. A* **2014**, *90*, 043403, https://doi.org/10.1103/PhysRevA.90.043403
[21] A. B. Henson, S. Gersten, Y. Shagam, J. Narevicius, E. Narevicius, *Science* **2012**, *338*, 234, https://doi.org/10.1126/science.1229141
[22] J. Jankunas, K. Jachymski, M. Hapka, A. Osterwalder, *J. Chem. Phys.* **2015**, *142*, 164305, https://doi.org/10.1063/1.4919369
[23] T. Halfmann, J. Koensgen, K. Bergmann, *Meas. Sci. Technol.* **2000**, *11*, 1510, https://doi.org/10.1088/0957-0233/11/10/312
[24] T. F. Gallagher, 'Rydberg Atoms', Cambridge University Press, Cambridge, **1994**.
[25] V. Zhelyazkova, M. Žeško, H. Schmutz, J. A. Agner, F. Merkt, *Mol. Phys.* **2019**, *117*, 2980, https://doi.org/10.1080/00268976.2019.1600060
[26] P. Langevin, *Ann. Chim. Phys.* **1905**, *T5*, 245.
[27] M. D. Marshall, K. C. Izgi, J. S. Muenter, *J. Chem. Phys.* **1997**, *107*, 1037, https://doi.org/10.1063/1.474479
[28] F. Daniel, C. Rist, A. Faure, E. Roueff, M. Gérin, D. C. Lis, P. Hily-Blant, A. Bacmann, L. Wiesenfeld, *Mon. Not. R. Astron. Soc.* **2016**, *457*, 1535, https://doi.org/10.1093/mnras/stw084
[29] Š. Urban, R. D'Cunha, K. Narahari Rao, D. Papoušek, *Can. J. Phys.* **1984**, *62*, 1775, https://doi.org/10.1139/p84-223

The definitive version of this article is the electronic one that can be found at https://doi.org/10.2533/chimia.2022.316